JCTC Journal of Chemical Theory and Computation

Adsorption and Diffusion of Alkanes in Na-MOR: Modeling the Effect of the Aluminum Distribution

Shuai Ban[†] and Thijs J. H. Vlugt*[,‡]

Condensed Matter and Interfaces, Department of Chemistry, Utrecht University, P.O. Box 80.000 3508TA Utrecht, The Netherlands and Delft University of Technology, Process & Energy Laboratory, Leeghwaterstraat 44, 2628CA Delft, The Netherlands

Received June 22, 2009

Abstract: We investigated the adsorption and the diffusion of alkanes in the sodium-exchanged zeolite Mordenite (Na-MOR) using molecular simulations. MOR-type zeolite consists of main channels (6.5 × 7 Å) oriented along the *z* crystallographic axis that are connected to small side pockets (3.4 × 4.8 Å). It is well-known that the adsorption of alkanes in Na-MOR strongly depends on the precise location of the framework Al atoms either in the main channel or the side pockets (Calero and co-workers, *Angew. Chem. Int. Ed.* **2007**, *46*, 276). We found that this effect can be characterized by a single-order parameter: the number of framework Al in the main channel divided by the number of framework Al in the side pocket (M/S ratio). For any M/S ratio, the adsorption isotherm follows from a linear interpolation between the reference isotherms. This enabled us to predict adsorption isotherms for any distribution of the Al framework atoms or estimate the M/S ratio for a given isotherm. We found that the same model can predict the effect of the M/S ratio on the self-diffusion coefficient, the Maxwell−Stefan diffusion coefficient, and the accessible micropore volume.

1. Introduction

Mordenite (MOR-type zeolite) is an important catalyst in the petrochemical industry, as it is used for the acid-catalyzed isomerization of alkanes and aromatics.[1,2] For example, Pt/H-MOR is a suitable catalyst for the hydro-isomerization of linear alkanes to branched ones, even though slow intracrystalline transport hinders the catalytic performance to some extent.[3] Therefore, it is important to understand the adsorption and transport of hydrocarbon molecules in this zeolite.[4] The framework of MOR-type zeolite consists of main channels formed by large 12-membered rings with an elliptical shape of 6.7 × 7.0 Å oriented along the *z* crystallographic axis. Small side pockets are connected to these main channels by eight-membered rings (3.4 × 4.8 Å) that are oriented along the *y* crystallographic axis.[5] It was found that methane is the only hydrocarbon that can be adsorbed in the side pockets.[6,7]

In general, the structure of zeolites consists of covalently bonded TO_4 units, in which the framework T atom is usually a silicon (Si) or an aluminum (Al) atom. To obey charge neutrality, the substitution of a Si atom by an Al atom requires the presence of a nonframework cation (usually Na^+ or K^+) or a proton (H^+). It is well-known that the adsorption of guest molecules in Na-MOR is significantly enhanced by nonframework Na^+ cations.[8] The positions of the nonframework cations in MOR-type zeolite are coupled to the positions of the framework Al atoms.[9] The *average* distribution of framework Al over the various T sites (labeled T_1, ..., T_4) in Na-MOR was obtained experimentally by detecting Brønsted acid sites.[9−12] It was found that the majority of Al is located at the T_3 and T_4 sites close to the side pockets. Knowledge on the distribution of Al among T sites alone is not sufficient to obtain the *exact* individual positions of all framework Al atoms. Recently, Calero and co-workers used an elegant reversed engineering approach to identify the positions of the framework Al atoms in zeolites.[13,14] For a fixed Si/Al ratio, this approach considers all possible

* Corresponding author. E-mail: t.j.h.vlugt@tudelft.nl.
[†] Utrecht University.
[‡] Delft University of Technology.

10.1021/ct900315r CCC: $40.75
Published on Web 09/14/2009

distributions of Al in the unit cell of the zeolite. It was found that this approach correctly predicts the Al distribution in Na-MOR. These authors also found that for some zeolites, e.g., LTA, FAU, and MFI, the precise positions of the framework Al atoms do not influence adsorption, while for other zeolites, e.g., MOR, FER, and TON, the adsorption strongly depends on the positions of the framework Al atoms. For MOR-type zeolite, this is because nonframework Na^+ cations in the side pocket only have a weak interaction with adsorbed guest molecules in the main channel, while this interaction is much stronger for cations located in the main channel.

Many experimental and simulation studies have investigated the effect of nonframework cations on the diffusivity of guest molecules, particularly in MFI-type zeolite.[15−18] Fan et al.[16] used molecular dynamics simulations to study the diffusion of ethene in MFI-type zeolite. These authors found that the diffusion of ethene was slowed down from 2.7×10^{-9} m^2/s in a silicalite framework to 1.6×10^{-9} m^2/s in ZSM-5 with four Al per one unit cell. Masuda et al.[18] studied the influence of acid sites on the diffusion of aromatics in MFI-type zeolite. This study revealed that at low temperatures, the diffusivity significantly decreased with an increasing number of acid sites, while the diffusion of aromatics was hardly affected by the acid sites at high temperatures. Leroy et al.[15] combined the quasi-elastic neutron-scattering technique with molecular simulations to study the diffusion of alkanes in MFI. These authors found that the diffusivity of octane in silicalite is four times larger than in Na-ZSM-5. This result agreed well with their molecular dynamics simulations for MFI-type zeolite with two Na^+ per unit cell. In summary, previous studies show that diffusion of hydrocarbons is slowed down by nonframework cations. Therefore, it is important to know the effect of the Al distribution on this.

In this work, computer simulations were used to investigate the influence of the positions of framework Al on the adsorption and diffusion properties of Na-MOR in a more coarse-grained way. In our simulations, the Al distribution was described by a single-order parameter: the M/S ratio, which is the ratio of the number of framework Al in the main channels (M) and the side-pockets (S) in MOR-type framework (M/S ratio). The reasons for using this order parameter were: (1) The adsorption of guest molecules is only sensitive to the framework Al located in either the main channels or the side pockets, rather than the exact positions of framework Al atoms. (2) The Al distribution is a more accessible parameter for experiments than the distribution of nonframework Na^+.

This paper is organized as follows. In Section 2, we briefly describe the construction of a Na-MOR supercell as well as the simulation methods for computing the adsorption isotherms, the diffusivities, and the accessible micropore volume. In Section 3.1, the computed Na^+ distribution in MOR is compared with experiments. In Section 3.2, we present an interpolation model to predict isotherms in Na-MOR for any M/S ratio, using two reference isotherms with a known M/S ratio. In Section 3.3, we show that the nonframework Na^+ cations seriously hinder the diffusion of alkanes in Na-MOR at low temperature, and this effect is correctly described by our model. We show that our model is also applicable for calculating the micropore volume of Na-MOR (Section 3.4). Our findings are summarized in Section 4.

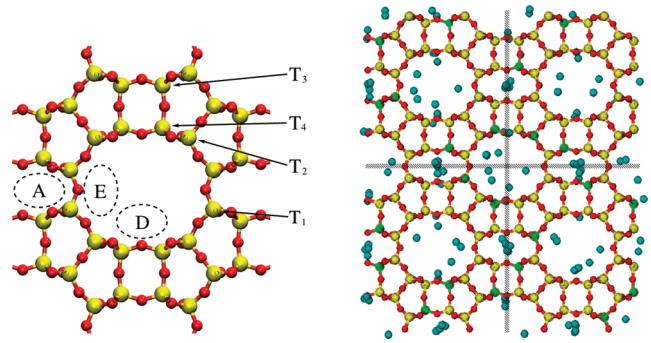

Figure 1. (a) The preferential sites A, D, and E for nonframework Na^+ cations in Na-MOR. The colors are: red for O and yellow for Si and Al. The four T sites T_1, T_2, T_3, and T_4 are shown as well. (b) Typical snapshot of Na-MOR with Si/Al = 5 for a supercell consisting of $2 \times 2 \times 4$ unit cells at 300 K. The colors are: red for O, cyan for Na^+, yellow for Si, and black for Al.

2. Simulation Methods

2.1. The Na-MOR Lattice. Zeolite Na-MOR consists of Na, Si, Al, and O atoms with the composition $Na_xAl_xSi_{48-x}O_{96}$. Natural mordenite has a Si/Al ratio of approximately 4.3−6.0, so $x \approx 8$.[10] Demuth et al.[19] pointed out that the most common space group for MOR-type zeolite is *Cmcm* with the exception of dehydrated protonated MOR which has space group *Pbcn*. Macedonia et al.[20] showed that differences in adsorption isotherms between the space groups *Cmcm* and *Pbcn* are negligible. Therefore, in this paper we restricted ourselves to the Na-MOR lattice with a *Cmcm* symmetry. The dimensions of the MOR unit cell are 18.094 × 20.516 × 7.524 Å with $\alpha = \beta = \gamma = 90°$. Each unit cell contains four different tetrahedral sites (T_1, ..., T_4) for Si and Al framework atoms, and ten different oxygen sites (O_1, ..., O_{10}).[21] The T_3 sites are located in the side pocket, while T_1, T_2, and T_4 are located in the main channel, see Figure 1a. Alberti et al.[10] derived the Al distribution over the four T sites in natural Na-MOR from X-ray diffraction (XRD) measurements. This is also expected to be applicable to synthetic Na-MOR and H-MOR.

In this work, we constructed large supercells of MOR-type zeolite consisting of $2 \times 2 \times 4$ unit cells. Starting from an all-silica supercell, Si framework atoms are randomly substituted by Al in such a way that (1) the Löwenstein rule is obeyed, and (2) the relative Al content of each T site corresponds to the given M/S ratio. As a result, many Na-MOR supercells could be generated with the same Si/Al ratio but with different positions of the framework Al. We will show that the properties of these supercells are nearly identical, as the relative Al content of the T sites in the main channel and the side pocket is identical for these supercells. Computed properties were then averaged over 5−10 supercells.

2.2. Computing Adsorption Isotherms. Adsorption isotherms were computed by using configurational-bias Mon-

te Carlo[22−24] simulations in grand-canonical ensemble (GCMC).[24−27] Interactions between the guest molecules, the zeolite framework, and the nonframework cations were described by Lennard-Jones interactions. In addition, electrostatic interactions between the nonframework Na^+ cations and the framework were included. All force field parameters were taken from the work of Calero et al.[28] The Ewald summation was used to compute electrostatic interactions. A typical simulation consisted of 3×10^6 Monte Carlo cycles. In each cycle, trial moves were chosen at random with a fixed probability: translation of a guest molecule or a nonframework cation (15%), rotation of a guest molecule (15%), exchange of a guest molecule with a particle reservoir (55%), and partial regrowth of a guest molecule (15%). The number of trial moves in each cycle was equal to the number of adsorbed guest molecules with a minimum of 20. The number of Na^+ atoms in Na-MOR was constant during the simulations. For the simulation of adsorption, the zeolite framework was kept rigid, and the nonframework cations were mobile. For the systems considered here, including framework flexibility usually results in a negligible deviation of adsorption isotherms.[29] For more details on these simulations, we refer the reader to refs 26−28.

2.3. Computing Diffusivities of Guest Molecules. Molecular dynamics simulations[30] were used to calculate the self- and Maxwell−Stefan diffusion coefficients of adsorbed guest molecules in MOR-type zeolite. We used the velocity Verlet algorithm[31] with a time step of 0.5 fs. The temperature was controlled by a Nosé−Hoover thermostat.[24] The initial configuration of guest molecules was taken from the final configuration of a Monte Carlo simulation in the NVT ensemble. To avoid single-file diffusion, each main channel of MOR-type zeolite contained only a single guest molecule. For simplicity, we used a rigid framework. Nonframework cations were allowed to move freely in the zeolite. The self- (D^{self}) and Maxwell−Stefan diffusion coefficients (D^{MS}) of a single component adsorbed in a zeolite were computed from particle displacements:

$$D_\alpha^{self} = \frac{1}{2n} \lim_{\Delta t \to \infty} \frac{1}{\Delta t} \left\langle \left(\sum_{i=1}^{n} (r_{i,\alpha}(t + \Delta t) - r_{i,\alpha}(t))^2 \right) \right\rangle \quad (1)$$

$$D_\alpha^{MS} = \frac{1}{2n} \lim_{\Delta t \to \infty} \frac{1}{\Delta t} \left\langle \left(\sum_{i=1}^{n} (r_{i,\alpha}(t + \Delta t) - r_{i,\alpha}(t)) \right)^2 \right\rangle \quad (2)$$

in which α is the direction of diffusion, n is the number of adsorbed guest molecules, and $r_i(t)$ is the position of molecule i at time t.[32−34] For MOR-type zeolite, only diffusion in the main channel (z direction) was taken into account, i.e., $\alpha = z$. In practice, the mean-square displacement in eqs 1 and 2 was computed using an order-n algorithm.[24,33,35]

2.4. Pore Size Distribution. In this work, the pore size of a certain cavity or channel was defined as the maximum diameter of a sphere that can be located in there. This definition is applicable to pores with an arbitrary shape. For cylindrical or slit pores, our definition is identical to the IUPAC definition.[36] Using this definition, the pore size distribution was computed from the coordinates of the framework atoms using the following algorithm:[37] (1) A three-dimensional grid with a small spacing is constructed. We typically use a grid size of 0.1 Å (in each direction). (2) A spherical test particle is positioned at a random position in the zeolite. The radius of this particle is chosen as the minimum distance between the center of the particle and any of the zeolite framework atoms minus the radius of the closest framework atom. The radius of an oxygen framework atom is 1.35 Å, and the radius is 0.99 Å for Na^+ .[21] Tetrahedral atoms, e.g. Si, Al, are not considered, as for most zeolites they are well screened by adjacent oxygen atoms.[38] (3) The diameter of the test particle is recorded for all grid points that are inside the spherical particle. (4) This procedure is repeated many times. We found that the number of test spheres should be at least 100 times the number of grid points. For each grid point, the maximum recorded diameter is computed, and this quantity is defined as the local pore size of a specific grid point. The simulation stops when the local pore size of all grid points is converged. (5) The fraction of pores with a diameter between r and $r + \Delta r$ (pore size distribution) is equal to the fraction of grid points with a maximum diameter between r and $r + \Delta r$. Using our calculated pore size distribution, the micropore volume was calculated by integrating the pore size distribution from 4.5 to 20 Å. For more details, we refer the reader to ref 37.

Table 1. Comparison of the Na^+ Occupancies between Experiments and Simulations

	Si/Al	site A, %	site D, %	site E, %
experiment[a]	5.7	43	36	21
experiment[b]	5.7	53	34	13
experiment[c]	5	49	32	19
simulation[d]	5	50	38	12
this work	5.0	40.2	35.5	20.9
this work	5.5	40.1	35.3	20.9

[a] Schlenker et al.[5] [b] Devautour et al.[41] [c] Coughlan et al.[39,44] [d] Tyburce et al.[45] The Na^+ occupancy was averaged over five supercells. Note that the differences in occupancy between the supercells were very small.

3. Results and Discussion

3.1. Na^+ Distribution. Nonframework Na^+ cations interact with the framework Al through Lennard-Jones and long-range Coulombic interactions. As a consequence, Na^+ cations are not directly bonded to framework Al atoms. Experiments on dehydrated Na-MOR crystals[5,39−41] identified three favorable locations for nonframework Na^+: the center of eight-membered rings that run parallel to the main channels (site A), the main channel at the entrance of the side pocket (site D), and the main channel far away from the side pocket (site E), see Figure 1a. Our simulations showed the same adsorption sites for Na nonframework cations, see Figure 1b. The Na^+ occupancies at these sites have been computed for natural Na-MOR with Si/Al = 5 and 5.5, respectively. Table 1 shows that the computed Na^+ occupancies at these sites agree very well with the available experiments. For different supercells with an identical distribution of Al over the T sites, we found that the occupancy of Na^+ at the three sites is nearly identical. The

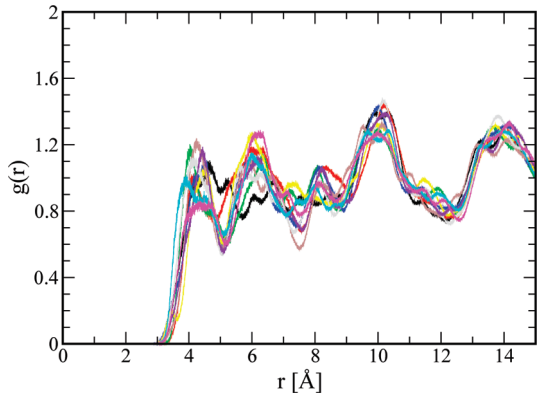

Figure 2. Radial distribution functions for Na^+-Na^+ interactions for 10 supercells with the same Al distribution (Si/Al = 5), see Section 2.1.

corresponding radial distribution functions for Na^+-Na^+ interactions are very similar, as they all show peaks at distances of 4.3, 6.2, 10.1, and 14 Å, see Figure 2.

3.2. Prediction of Adsorption Isotherms. Na-MOR has two main adsorption sites for alkanes, the large main channels and the smaller side pockets. Methane is the only alkane that can access the side pockets.[6,7] The side pockets are also accessible for nonframework Na^+ cations. It is natural to divide the nonframework Na^+ cations into two groups: Na^+ in the main channels (denoted by Na_M^+) and Na^+ in the side pockets (denoted by Na_S^+). Na_M^+ corresponds to the Na^+ cations at site D and E, while Na_S^+ corresponds to Na^+ at site A. The Na_M^+ cations interact more strongly with alkanes absorbed in the main channel, as they are more close by. A convenient order parameter to characterize the Na^+ distribution is the Al M/S ratio, which is the ratio of the number of the framework Al in the main channels and the side pockets. The reason for this is that, due to the strong interactions between Al and Na^+, the distribution of the Na^+ cations approximately follows that of the framework Al. The difference of the adsorption properties between different Na-MOR supercells with the same Al M/S ratio was found to be small in our simulations. Al framework atoms at the crystallographic site T_3 are considered to be in the side pocket, while Al atoms at T_1, T_2, and T_4 are considered to be in the main channel, see Figure 1a. The same classification was previously used by IR spectroscopy experiments of probe molecules in MOR-type zeolite.[42] This technique is used to locate Brønsted acid sites in H-MOR. We expect that the Al distribution in Na-MOR is the same as in H-MOR, as H-MOR is usually obtained by exchanging Na^+ with H^+.[43]

To model the adsorption behavior of alkanes in Na-MOR, as a function of the M/S ratio (Al content in the main channel divided by the Al content in the side pocket, here denoted by r), we constructed the following model. The total number of Al atoms per unit cell is denoted by n, while n_M and n_S are the number of Al atoms per unit cell in the main channels and the side pockets, respectively. Of course:

$$n = n_M + n_S \tag{3}$$

and we define the ratio r by

$$r = \frac{n_M}{n_S} \tag{4}$$

From this it directly follows that:

$$n_M = n\frac{r}{r+1} \tag{5}$$

$$n_S = n\frac{1}{r+1} \tag{6}$$

Our key assumption is that the loading of guest molecules at pressure P (here denoted by $I(P)$) is a linear function of n_M and n_S:

$$\begin{aligned} I(P) &= I_0(P) + \alpha_M(P)n_M + \alpha_S(P)n_S \\ &= I_0(P) + \frac{n}{r+1}[\alpha_M(P)r + \alpha_S(P)] \end{aligned} \tag{7}$$

where $\alpha_M(P)$ and $\alpha_S(P)$ are pressure-dependent constants and $I_0(P)$ is the loading of guest molecules for all-silica MOR at pressure P. The maximum number of Al at the T_3 sites is four Al atoms per unit cell ($n_S \leq 4$), which is much lower than the maximum possible number of Al in the main channel. For a given total content of framework Al atoms, there are two extreme situations: (1) the M structure, i.e., all Al is located in main channels ($n_S = 0$, $n_M = n$, the corresponding adsorption isotherm is denoted by $I_M(P)$) and (2) the S structure, where the side pockets are fully loaded with Al, and the remaining Al are located in the main channel (adsorption isotherm denoted by $I_S(P)$). This leads to

$$I_M(P) = I_0(P) + \alpha_M(P)n \tag{8}$$

and

$$I_S(P) = \begin{cases} I_0(P) + \alpha_S(P)n & \text{for} \quad n \leq 4 \\ I_0(P) + 4\alpha_S(P) + (n-4)\alpha_M(P) & \text{for} \quad n > 4 \end{cases} \tag{9}$$

By eliminating $\alpha_M(P)$ and $\alpha_S(P)$ we obtain

$$I(P) = \begin{cases} \frac{r}{r+1}I_M(P) + \frac{1}{r+1}I_S(P) & \text{for} \quad n \leq 4 \\ \frac{4r-n+4}{4(r+1)}I_M(P) + \frac{n}{4(r+1)}I_S(P) & \text{for} \quad n > 4 \end{cases} \tag{10}$$

When the Si/Al ratio is larger than 11 (i.e., $n \leq 4$), the weight factors of $I_M(P)$ and $I_S(P)$ in eq 10 are simply the fractions of framework Al at the sites M and S.

To test the prediction of eq 10, we computed adsorption isotherms of propane and butane in Na-MOR. These molecules are exclusively adsorbed in the main channels. Figure 3 shows the computed adsorption isotherms I_M and I_S for Na-MOR with four Al per unit cell. Both isotherms significantly differ from the one for an all-silica structure. As expected, the adsorption isotherm strongly depends on the positions of the framework Al atoms, and the differences between isotherms of different supercells are small. At a given pressure, the adsorbed amount for the S structure is always lower than that of the M structure due to the increased average distance between the guest molecules and the nonframework Na^+ cations.

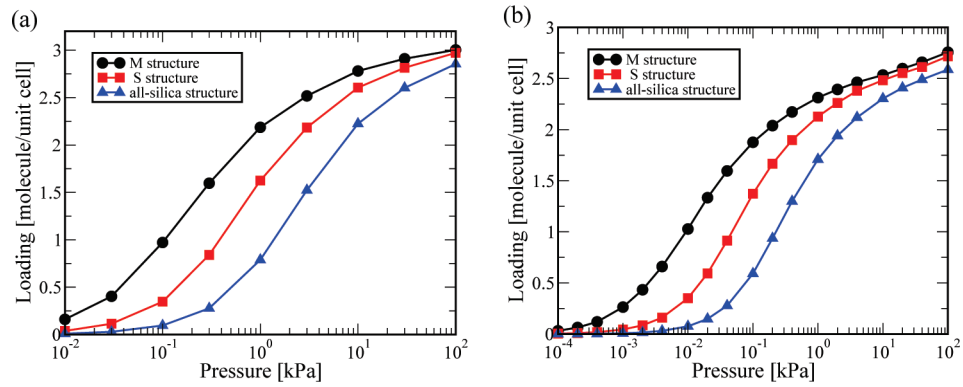

Figure 3. Adsorption isotherms of propane (a) and butane (b) in Na-MOR at 300 K for Si/Al = 11. The M and S structures are shown as well as the isotherm for the all-silica structure. Each isotherm is the average over three supercells with the same M/S ratio. The error bars indicate the differences between these supercells. For each supercell, the error in the computed loading is much smaller than the symbol size.

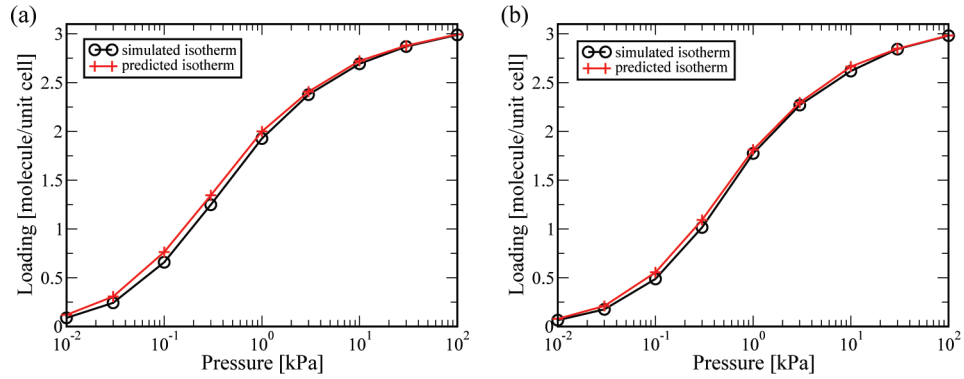

Figure 4. Linear interpolation of adsorption isotherms for propane in Na-MOR with Si/Al = 11 at 300 K. The predicted isotherm using eq 9 was compared to the computed isotherm at the same Al M/S ratio. (a) Al M/S ratio 2:1 and (b) Al M/S ratio 1:2.

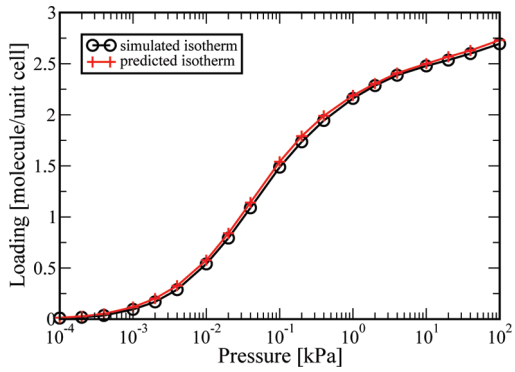

Figure 5. Linear interpolation of adsorption isotherms for butane in Na-MOR with Si/Al = 11 at 300 K. The predicted isotherm using eq 10 was compared to the computed isotherm at the same Al M/S ratio 1:2.

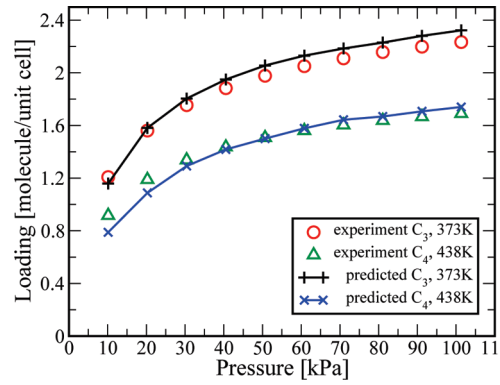

Figure 6. Comparison of the predicted isotherms (eq 10) with experimental data[7] for propane and butane in Na-MOR with Si/Al = 19.75 at 373 and 438 K. The estimated Al M/S ratio was 3:1 for this system.

Figures 4 and 5 show that the prediction of eq 10 is excellent. This result is useful in two ways: First, the adsorption isotherm for an arbitrary M/S ratio can be predicted by linear interpolation between two reference isotherms (for which we know the M/S ratio). Second, the M/S ratio in a Na-MOR sample can be estimated by fitting a measured isotherm to two reference isotherms. As an example, we estimated an M/S ratio of 3:1 from experimental adsorption isotherms of propane and butane in Figure 6. This estimated ratio is close to the ratio of 2:1 proposed by Alberti et al.[10]

In Figure 7, it is shown that our interpolation model is able to accurately predict the Henry coefficients of *n*-alkanes with 2−5 carbon atoms. For longer *n*-alkanes, small differences appeared between the computed and the predicted Henry coefficients. The reason for this is that longer chains will have interactions with more Na^+ cations at the same time, leading to nonlinear effects.

3.3. Prediction of Diffusivities. The computed and predicted diffusivities of alkanes in Na-MOR for various Si/Al ratios are shown in Table 2. The simulations were performed for propane and hexane diffusing in the all-silica MOR and

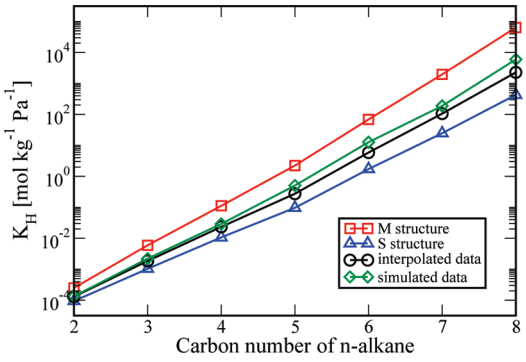

Figure 7. Linear interpolation of the Henry coefficients of *n*-alkanes in Na-MOR with Si/Al = 11 at 300 K. The error bars are much smaller than the symbols.

Table 2. Self- and Maxwell−Stefan Diffusion Coefficients of Propane and Hexane in All-Silica MOR and Na-MOR with Si/Al = 5:23 at 300 K and 600 K[a]

	Si/Al	C_3 at 300 K	C_6 at 300 K	C_3 at 600 K	C_6 at 600 K
D^{self}	∞	5.5	7.0	12.3	13.1
D^{self}	23	2.5	1.6	7.0	5.7
D^{self}	5	1.8	0.9	5.5	3.6
D^{MS}	∞	5.5	7.0	11.6	12.8
D^{MS}	23	2.3	1.4	6.9	5.5
D^{MS}	5	1.8	0.9	5.3	3.5

[a] Each main channel contained a single alkane molecule. Self- and Maxwell−Stefan diffusivities are denoted by D^{self} and D^{MS} in units of 10^{-8} m^2/s, respectively. The diffusion coefficients in Na-MOR were obtained by averaging over 10 supercells with the same M/S ratio. The differences between supercells are approximately 15%. For each supercell, the error in the computed diffusivity was around 20% for D^{MS} and 10% for D^{self}. For all-silica MOR, the error in the computed diffusion coefficients was smaller than 1%.

Na-MOR containing two or eight Na^+ cations at 300K and 600K, respectively. As each main channel contains a single alkane molecule only, it is expected that the Maxwell−Stefan and the self-diffusivities do not differ very much. It can be seen from Table 2 that both the self- and Maxwell−Stefan diffusivities decrease as a function of the Na^+ concentration irrespective of the temperature and the alkane chain length. This is in line with the results from Leroy et al.[15] Note that the differences of the calculated diffusivities were about 15% for supercells with the same Al distribution. For each supercell, the simulation error is about 20% for D^{MS} and 10% for D^{self}. These errors are much smaller than the difference of the diffusivities for Na-MOR with different Si/Al ratios. Therefore, we can conclude that the diffusion of alkanes is slowed down by the nonframework cations of Na-MOR.

The self- and Maxwell-Stefan diffusivities were computed for propane in Na-MOR with Si/Al = 11 at 300 K and 600 K at a loading of one propane per main channel, see Table 3. As the loading is quite low, the self- and Maxwell−Stefan diffusivities are almost equal. However, the diffusivity of propane in the S structure is more than twice as large as in the M structure. The reason for this is that because of the strong interactions between propane and Na^+, the Na^+ ions in the main channels will slow down the diffusion of propane significantly. Therefore, $D_M < D_{M/S = 2:1} < D_{M/S = 1:2} < D_S$. In the same spirit as eq 10, we predicted the self- and

Table 3. Interpolation of Propane and Hexane Diffusivities in Na-MOR with Si/Al = 11 at 300 K and 600 K, Respectively[a]

		D_M	D_S	$D_{M/S = 1:2}$	$D_{M/S = 2:1}$
		C_3 (300 K)			
simulated	D^{self}	1.4	2.8	2.0	1.6
predicted	D^{self}	n.a.	n.a.	2.3	1.9
simulated	D^{MS}	1.3	3.0	2.2	1.4
predicted	D^{MS}	n.a.	n.a.	2.4	1.9
		C_6 (600 K)			
simulated	D^{self}	3.1	5.1	4.5	3.7
predicted	D^{self}	n.a.	n.a.	4.4	3.8
simulated	D^{MS}	2.9	5.1	4.6	3.5
predicted	D^{MS}	n.a.	n.a.	4.4	3.6

[a] Each main channel contained a single alkane molecule. Self- and Maxwell−Stefan diffusivities were denoted by D^{self} and D^{MS} in units of 10^{-8} m^2/s. D_M and D_S are the computed diffusivities for the M and S structure, see Section 3.2. All reported values were obtained by averaging over 10 supercells with the same M/S ratio. The differences between supercells are approximately 12%. For each supercell, the error in the estimated diffusivity was approximately 20% for D^{MS} and 5% for D^{self}.

Table 4. Interpolation of the Micropore Volume (V) of Na-MOR with Si/Al = 11 in Units of mL/g[a]

	V_M	V_S	$V_{M/S = 1:2}$	$V_{M/S = 2:1}$
simulated	0.1816	0.1934	0.1874	0.1855
predicted	n.a.	n.a.	0.1894	0.1855

[a] The notation is the same as in Table 3. All values were obtained by averaging over 10 supercells with the same Al M/S ratio. The differences of the micropore volumes were 0.5% for the 10 supercells with the same Al M/S ratio. The simulation error of the micropore volume for each supercell was approximately 0.2%.

Maxwell−Stefan diffusivities for M/S = 2:1 and M/S = 1:2, based on the computed diffusivities D_M and D_S:

$$D = \begin{cases} \dfrac{r}{r+1}D_M + \dfrac{1}{r+1}D_S & \text{for} \quad n \le 4 \\ \dfrac{4r-n+4}{4(r+1)}D_M + \dfrac{n}{4(r+1)}D_S & \text{for} \quad n > 4 \end{cases} \tag{11}$$

In this equation, D is the predicted diffusivity and D_M and D_S are the two reference diffusivities. The predicted diffusivities are very close to the computed ones. Differences of calculated diffusivities are about 12% for the supercells with the same Al M/S ratio. For each supercell, the simulation error is about 20% for D^{MS} and 5% for D^{self}. These errors are much smaller than the difference of the diffusivities for Na-MOR with different Al M/S ratios. Therefore, we can conclude that the interpolation scheme is able to predict self- and Maxwell−Stefan diffusivities in Na-MOR.

3.4. Prediction of the Micropore Volume. The micropore volume of Na-MOR for different M/S ratios is shown in Table 4. As the micropore volume was calculated from pores in the range of 4.5−20 Å, the main contribution to the micropore volume originates from the main channels. Therefore, when all the nonframework Na^+ is located in the main channel, the micropore volume decreases. This leads to the following prediction: $V_M < V_{M/S = 2:1} < V_{M/S = 1:2} < V_S$. For a given M/S ratio, the micropore volume can be computed using

$$V = \begin{cases} \frac{r}{r+1}V_M + \frac{1}{r+1}V_S & \text{for} \quad n \leq 4 \\ \frac{4r-n+4}{4(r+1)}V_M + \frac{n}{4(r+1)}V_S & \text{for} \quad n > 4 \end{cases} \tag{12}$$

Table 4 shows that the predicted micropore volumes are in good agreement with the computed ones. The differences in micropore volume are 0.5% for supercells with the same M/S ratio. The error in the computed micropore volume for each supercell is about 0.2%. These errors are more than 1 order of magnitude smaller than the difference in the micropore volume between the M and S structure. Therefore, we can conclude that the interpolation scheme works also well for the prediction of the accessible micropore volume in Na-MOR.

4. Conclusions

We presented a simple interpolation model to predict the effect of the framework Al distribution on the adsorption isotherms and diffusivities of alkanes in Na-MOR as well as the micropore volume. The key parameter is the Al M/S ratio, which is the ratio between the number of Al atoms in the side pockets (T_3 sites) and the main channels (T_1, T_2, and T_4 sites). Our model predictions match the computed values very well.

Acknowledgment. The authors acknowledge funding from the ACTS/ASPECT Program from The Netherlands Organization for Scientific Research (NWO−CW). T.J.H. Vlugt acknowledges financial support from NWO−CW through a VIDI grant.

References

(1) Lee, G. J.; Graces, J. M.; Meima, G. R.; Van der Aalst, M. J. M. *U.S. Patent* 5,198,595, 1991.

(2) Tromp, M.; van Bokhoven, J. A.; Oostenbrink, M. T. G.; Bitter, J. H.; de Jong, K. P.; Koningsberger, D. C. *J. Catal.* **2000**, *190*, 209–214.

(3) Leia, G. D.; Carvilla, B. T.; Sachtler, W. M. H. *Appl. Catal. A Gen.* **1996**, *142*, 347–359.

(4) Haag, W. O. In *Zeolites and Related Microporous Materials: State of the Art 1994, Studies in Surface Science and Catalysis*; Weitkamp, J., Karge, H. G., Pfeifer, H., Hölderich, W., Eds.; Elsevier: Amsterdam, The Netherlands, 1994; Vol. 84, pp. 1375−1394.

(5) Schlenker, J. L.; Pluth, J. J.; Smit, J. V. *Mater. Res. Bull.* **1979**, *14*, 751.

(6) Choudhary, V. R.; Mayadevi, S.; Singh, A. P. *J. Chem. Soc. Faraday Trans.* **1995**, *91*, 2935–2944.

(7) Webster, C. E.; Cottone, A.; Drago, R. S. *J. Am. Chem. Soc.* **1999**, *121*, 12127–12139.

(8) Beerdsen, E.; Dubbeldam, D.; Smit, B.; Vlugt, T. J. H.; Calero, S. *J. Phys. Chem. B* **2003**, *107*, 12088–12096.

(9) Marie, O.; Massiani, P.; Thibault-Starzyk, F. *J. Phys. Chem. B* **2004**, *108*, 5073–5081.

(10) Alberti, A. *Zeolites* **1997**, *19*, 411–415.

(11) Niwa, M.; Suzuki, K.; Katada, N.; Kanougi, T.; Atoguchi, T. *J. Phys. Chem. B* **2005**, *109*, 18749–18757.

(12) Bevilacqua, M.; Busca, G. *Catal. Commun.* **2002**, *3*, 497–502.

(13) García-Pérez, E.; Dubbeldam, D.; Liu, B.; Smit, B.; Calero, S. *Angew. Chem., Int. Ed.* **2007**, *46*, 276–278.

(14) Liu, B.; García-Pérez, E.; Dubbeldam, D.; Smit, B.; Calero, S. *J. Phys. Chem. C* **2007**, *11*, 10419–10426.

(15) Leroy, F.; Jobic, H. *Chem. Phys. Lett.* **2005**, *406*, 375–380.

(16) Fan, J. F.; van de Graaf, B.; Xiao, H. M.; Njo, S. L. *J. Mol. Struct.* **1999**, *492*, 133–142.

(17) Fan, J. F.; Wang, Q. X.; Gong, X. D.; Xiao, H. M. *J. Mol. Struct.* **2003**, *638*, 129–134.

(18) Masuda, T.; Fujikata, Y.; Nishida, T.; Hashimoto, K. *Microporous Mesoporous Mater.* **1998**, *23*, 157–167.

(19) Demuth, T.; Hafner, J.; Benco, L.; Toulhoat, H. *J. Phys. Chem. B* **2000**, *104*, 4593–4607.

(20) Macedonia, M. D.; Moore, D. D.; Maginn, E. J.; Olken, M. M. *Langmuir* **2000**, *16*, 3823–3834.

(21) Baerlocher, C.; McCusker, L. B.; Olson, D. H. *Atlas of Zeolite Framework Types*, 6th ed.; Elsevier: Amsterdam, The Netherlands, 2007.

(22) Siepmann, J. I.; Frenkel, D. *Mol. Phys.* **1992**, *75*, 59–70.

(23) Siepmann, J. I. In *Computer Simulation of Biomolecular Systems: Theoretical and Experimental Applications*; van Gunsteren, W. F., Weiner, P. K., Wilkinson, A. J., Ed.; Escom Science Publisher; Leiden, The Netherlands, 1993; pp. 249−264.

(24) Frenkel, D.; Smit, B. *Understanding Molecular Simulation: from Algorithms to Applications*, 2nd ed. Academic Press: San Diego, CA, 2002.

(25) Smit, B. *Mol. Phys.* **1995**, *85*, 153–172.

(26) Vlugt, T. J. H.; Krishna, R.; Smit, B. *J. Phys. Chem. B* **1999**, *103*, 1102–1118.

(27) Dubbeldam, D.; Calero, S.; Vlugt, T. J. H.; Krishna, R.; Maesen, T. L. M.; Smit, B. *J. Phys. Chem. B* **2004**, *108*, 12301–12313.

(28) Calero, S.; Dubbeldam, D.; Krishna, R.; Smit, B.; Vlugt, T. J. H.; Denayer, J. F. M.; Martens, J. A.; Maesen, T. L. M. *J. Am. Chem. Soc.* **2004**, *126*, 11377–11386.

(29) Vlugt, T. J. H.; Schenk, M. *J. Phys. Chem. B* **2002**, *106*, 12757–12763.

(30) Rapaport, D. C. *The Art of Molecular Dynamics Simulation*, 2nd ed.; Cambridge University Press: Cambridge, U.K., 2004.

(31) Swope, W. C.; Andersen, H. C.; Berens, P. H.; Wilson, K. R. *J. Chem. Phys.* **1982**, *76*, 637–649.

(32) Krishna, R. *Chem. Phys. Lett.* **2000**, *326*, 477–484.

(33) Dubbeldam, D.; Snurr, R. Q. *Mol. Sim.* **2007**, *33*, 305–325.

(34) Smit, B.; Maesen, T. L. M. *Chem. Rev.* **2008**, *108*, 4125–4184.

(35) Dubbeldam, D.; Ford, D. C.; Ellis, D. E.; Snurr, R. Q. *Mol. Simul.* **2009**; doi: 10.1080/08927020902818039.

(36) Rouquerol, J.; Avnir, D.; Fairbridge, C. W.; Everett, D. H.; Haynes, J. H.; Pernicone, N.; Ramsay, J. D. F.; Sing, K. S. W. *Pure Appl. Chem.* **1994**, *66*, 1739–1758.

(37) Ban, S.; Vlugt, T. J. H. *Mol. Simul.* **2009**; doi: 10.1080/08927020802660614.

(38) Smit, B.; den Ouden, C. J. J. *J. Phys. Chem.* **1988**, *92*, 7169–7171.

(39) Coughlan, B.; Caroll, W. M.; Mcann, W. A. *J. Chem. Soc. Faraday Trans.* **1977**, *73*, 1612.

(40) Mortier, W. J. *Compilation of Extraframework Sites in Zeolites*; Butterworth: Guildford, U.K., 1982.

(41) Devautour, S.; Adboulaye, A.; Giuntini, J. C.; Henn, F. *J. Phys. Chem. B* **2001**, *105*, 9298–9301.

(42) Nesterenko, N. S.; Thibault-Starzyk, F.; Montouillout, V.; Yuschenko, V. V.; Fernandez, C.; Gilson, J. P.; Fajula, F.; Ivanova, I. I. *Microporous Mesoporous Mater.* **2004**, *71*, 157–166.

(43) Katada, N.; Takeguchi, T.; Suzuki, T.; Fukushima, T.; Inagaki, K.; Tokunaga, S.; Shimada, H.; Sato, K.; Oumi, Y.; Sano, T.; Segawa, K.; Nakai, K.; Shoji, H.; Wu, P.; Tatsumi, T.; Komatsu, T.; Masuda, T.; Domen, K.; Yoda, E.; Kondo, J. N.; Okuhara, T.; Kageyama, Y.; Niwa, M.; Ogura, M.; Matsukata, M.; Kikuchi, E.; Okazaki, N.; Takahashi, M.; Tada, A.; Tawada, S.; Kubota, Y.; Sugi, Y.; Higashio, Y.; Kamada, M.; Kioka, Y.; Yamamoto, K.; Shouji, T.; Arima, Y.; Okamoto, Y.; Matsumoto, H. *Appl. Catal. A Gen.* **2005**, *283*, 63–74.

(44) Pamba, M.; Maurin, G.; Devautour, S.; Vanderschueren, J.; Giuntini, J. C.; Renzo, F. D.; Hamidi, F. *Phys. Chem. Chem. Phys.* **2000**, *2*, 2027–2031.

(45) Tyburce, B.; Kappenstein, C.; Cartraud, P.; Garnier, E. *J. Chem. Soc. Faraday Trans.* **1991**, *87*, 2849–2853.

CT900315R